Desalination and Water Treatment
www.deswater.com

doi: 10.5004/dwt.2019.23694

152 (2019) 366–373
June

Adsorption of purpurin dye from industrial wastewater using Mn-doped Fe_2O_4 nanoparticles loaded on activated carbon

Masoumeh Kiani[a,*], Saideh Bagheri[a,*], Nima Karachi[b], Ebrahim Alipanahpour Dil[c]

[a]*Department of Chemistry, Payam Noor University, P.O. Box 19395-3697, Tehran, Iran, emails: M.Kiani@pnu.ac.ir (M. Kiani), S_bagheri2010@yahoo.com (S. Bagheri)*
[b]*Department of Chemistry, Marvdasht Branch, Islamic Azad University, Marvdasht, Iran, email: nimakarachi@miau.ac.ir*
[c]*Department of Chemistry, Yasouj University, Yasouj 75918-74831, Iran, email: e313ad@gmail.com*

Received 14 June 2018; Accepted 27 December 2018

ABSTRACT

Mn–Fe_2O_4 nanoparticles loaded on activated carbon were applied for removal of purpurin dye of solution. The effects of the amount of nanoparticles, pH of the solution, concentration of purpurin, and contact time were studied. The experiments have been designed by response surface methodology. The optimality conditions in the present study were 24 mg L^{-1} of purpurin concentration, 0.027 g adsorbent mass, pH value of 4.0, and 3.0 min of contact time. The artificial neural network model was employed for data prediction with Levenberg–Marquardt algorithm, purelin or a linear transfer function at output layer, and tansig or a tangent sigmoid transfer function in the hidden layer with 15 neurons. Remarkably, the experimental data and the pseudo-second-order kinetics fitted well. The isotherm analysis revealed that the equilibrium data were well fitted to the Langmuir isotherm model with the highest adsorption capacity of 60 mg g^{-1} of the adsorbent for removal of purpurin.

Keywords: Adsorption; Purpurin dye; Mn-doped Fe_2O_4 nanoparticles; Isotherm and kinetic

1. Introduction

Discharge of wastewater from textile industries into the environment is a serious environmental issue. Blanching of their high color and organic concentrations is laborious [1]. Since early antiquity, purpurin (1,2,4-trihidroxy anthraquinone) has been utilized in anthraquinone dyes like alizarin and purpurin which are released specifically by textile industries in the aquatic ecosystems and are intractable and persistent pollutants [2]. Coagulation–flocculation [3], aerobic or anaerobic treatment [4], electrochemical treatment [5], membrane filtration [6], and adsorption methods [7] are, by and large, used for treating dye wastewater. However, adsorption, owing to its effectiveness and the simplicity of the process, is the most well-liked among the methods. Moreover, a useful conjunction of adsorption methods with other effective processes like nanostructure and ultrasound are proved in increasing the efficiency and decreasing the cost of pollutant adsorption [8–10].

Different potential adsorbents have been utilized for the removal of specified organics from water samples. In this regard, magnetic nanoparticles have extensively been applied as novel adsorbents with large surface area, high adsorption capacity, and small diffusion resistance. As an illustration, they have been used for separation of chemical species like environmental pollutants, dyes, metals, and gases [11–15]. Applying spectrophotometry as the commonest approach for dye monitoring suffers from accuracy with overlapping peaks in the mixtures [16,17]. Therefore, derivative spectrophotometry has attracted the attention as an effective technique for overcoming this limitation and analyzing the dye concentration [18,19]. The wearisome and

* Corresponding authors.

exorbitant traditional optimization protocol by changing each single variable and investigating response suffers from the limitations of not providing suitable information about variable interaction and a distinct equation which results in response correlation to a significant term [20,21]. Because of the abovementioned drawbacks, statistical simultaneous optimization in response surface methodology (RSM) and in central composite design (CCD) as high-quantity tools have been chosen to provide such requirements [19,22–24]. Recently, the studies by the research groups have brought to light the fact that sonication has a significant contribution in decreasing the adsorption time and increasing the contact of samples with the adsorbent which can bring better mass transfer to the internal and external area and porosity of adsorbent [25,26]. Both RSM and the artificial neural network (ANN) have extensively been utilized in several fields for optimization of variables [27–32]. It is noteworthy that ultrasonic-assisted adsorption is a well-liked technique owing to its advantages over other conventional techniques [33]. In the adsorption of marked compounds from wastewater, ultrasonic-assisted adsorption method has extensively been applied [34]. This method demonstrates several considerable improvements in the adsorption process as it first necessitates much lower amount of adsorbent, then reduces adsorption time, and then increases adsorption efficiency [25,35]. Accordingly, the current study is based on the use of Mn–Fe_2O_4 nanoparticles loaded on activated carbon (Mn–Fe_2O_4–NPs–AC) under disparate operating conditions like adsorbent mass, pH, and sonication time for successful removal of purpurin. By using CCD under RSM, the parameters for maximum adsorption efficiency were optimized. By X-ray diffraction (XRD) and field emission scanning electron microscopy (FE-SEM), the structure and properties of the adsorbent were examined. Additionally, investigations on the adsorption kinetics and isotherms of dye removal of this sorbent were also performed. Furthermore, at optimum operational conditions, adsorption follows Langmuir with satisfying adsorption capacity and equilibrium data to describe the leading interactive mechanisms of the adsorption process.

2. Experimental

2.1. Reagents

Purpurin (Colour Index Number: 58205) was purchased from Acros Organics (Geel, Belgium). Sodium hydroxide, hydrochloric acid, $FeCl_3{\cdot}6H_2O$, active carbon, and $MnCl_2{\cdot}4H_2O$ were purchased from Merck, Darmstadt, Germany. Preparation of a stock solution of purpurin was done by dissolving 10 mg of purpurin in distilled water to achieve a concentration of 100 mg L^{-1} (100 mL) solution. All the characterization applied in this research for the adsorbent prepared were fully described in our previous publication [36].

2.2. Apparatus

For recording the visible spectra and absorbance measurements (λ_{max} = 470 nm), A ultraviolet visible (UV-Vis) spectrophotometer model Pharmacia Ultraspec 4000, equipped with a 1-cm quartz cell, was employed. FE-SEM (Hitachi S-4160, Japan) was also employed. The XRD measurements were carried out on an XRD Bruker D8 Advance. On a Shimadzu Fourier transform infrared (FTIR) 8000 spectrometer, the FTIR spectra were recorded. A pH meter (Metrohm model-728) was adjusted for the pH measurement. Ultrasonic Homogenizer (UHP-400), which was made in Ultrasonic Technology Development Company, Iran, was utilized for the ultrasound-assisted adsorption. All measurements were carried out at ambient temperature.

2.3. Statistical analysis

With the help of STATISTICA 10.0 software (State-Ease Inc., Minneapolis, USA), the experimental results of the CCD were investigated. Also for modeling and optimizing the impact of initial purpurin concentration (X_1), pH (X_2), amount of adsorbent (X_3), and contact time (X_4) on the ultrasonic-assisted adsorption of purpurin by Mn–Fe_2O_4–NPs–AC, RSM was employed. In Tables 1 and 2, the *R*% of purpurin for four independent variables which were set at five levels is shown. In order to assess the main and effective terms for modelling, the response based on *F*-test and *P*-values, analysis of variance (ANOVA) was performed [37,38].

2.4. Batch sorption experiments

In order to evaluate the impact of sonication time, adsorbent mass, pH, and initial purpurin concentration under RSM-based CCD on purpurin adsorption, 0.015–0.035 g Mn–Fe_2O_4 nanoparticles loaded on activated carbon were added into 50 mL purpurin solutions with different concentrations and pH for a predetermined sonication time at 25°C. In order to study these factors, sonication time in the range of 2.0–6.0 min, pH in the range of 2.0–10.0, and initial concentration of purpurin in the range of 10–30 mg L^{-1}were considered. To investigate the maximum adsorption of purpurin, 0.027 g adsorbent with a

Table 1
Process variables and their level for the purpurin adsorption by CCD

Factors	levels			Star point α = 2.0	
	Low (–1)	Central (0)	High (+1)	$-\alpha$	$+\alpha$
Purpurin concentration (mg L^{-1}) (X_1)	10	15	20	5	25
pH (X_2)	5.0	6.0	7.0	4.0	8.0
Adsorbent mass (g) (X_3)	0.0150	0.0225	0.0300	0.005	0.045
Sonication time (min) (X_4)	3.0	4.0	5.0	2.0	6.0

Table 2
The design matrix and the response

Run	X_1	X_2	X_3	X_4	R% purpurin
1	20	8	0.03	5	100.0
2	30	4	0.02	5	98.36
3	25	6	0.015	4	97.84
4	25	6	0.025	2	99.76
5	20	4	0.03	5	100.0
6	30	8	0.02	3	97.0
7	25	6	0.025	4	99.52
8	25	6	0.025	6	100.0
9	25	6	0.025	4	100.0
10	25	2	0.025	4	100.0
11	20	4	0.02	3	100.0
12	25	6	0.025	4	100.0
13	30	4	0.03	5	100.0
14	20	8	0.02	3	99.0
15	20	4	0.03	3	100.0
16	20	4	0.02	5	99.58
17	25	6	0.025	4	99.19
18	30	4	0.03	3	100.0
19	15	6	0.025	4	100.0
20	20	8	0.02	5	100.0
21	25	6	0.025	4	99.0
22	30	8	0.03	3	98.0
23	25	6	0.025	4	98.65
24	30	4	0.02	3	98.5
25	35	6	0.025	4	97.0
26	30	8	0.02	5	97.64
27	20	8	0.03	3	100.0
28	25	6	0.035	4	100.0
29	30	8	0.03	5	99.21
30	25	10	0.025	4	98.39

concentration of 24 mg $L^{-1}$and pH of 4.0 was added to purpurin solutions and agitated at 25°C for 3 min. After being centrifuged at 3,000 rpm for 15 min, the final concentration of purpurin in the supernatant was determined by utilizing an UV-Vis spectrophotometer (V-530, Jasco, Japan) at a wavelength of 470 nm (maximum absorbance). The adsorption percentage of purpurin dye (R% purpurin) and also the capacity for the adsorption of purpurin dye (q_i, mg/g) were calculated:

$$R\% = \frac{C_0 - C_e}{C_0} \times 100 \quad (1)$$

$$q_i = \frac{V\left(C_0 - C_e\right)}{M} \times 100 \quad (2)$$

C_0 and C_e in the formula are the initial and equilibrium concentrations of purpurin (mg L^{-1}), V stands for the volume of the solution (L), and M is the mass of the adsorbent used (g).

2.5. Artificial neural network

Feed forward back propagation (FFBP) was utilized as the training algorithm in this ANN. The ultimate calculated data for FFBP were compared with the experimentally obtained results, and subsequently, the errors were calculated and propagated backward and then employed for adjusting each neuron weight. All through the adsorption process, the input variables purpurin concentrations, adsorbent amount, and contact time were studied, and in this respect, 30 experimental points were employed to feed the model. From training, test, and validation sets which contained 60%, 20%, and 20% data points, respectively, the data set was originated. Based on Eq. (3), all of the data points were normalized in the range of [0.1, 0.9] owing to the use of tan-sigmoidal transfer function as follows [35]:

$$y = 0.8\left(\frac{X - X_{\min}}{X_{\max} - X_{\min}}\right) + 0.1 \quad (3)$$

X in the formula is a variable, while $X_{\min}$ is the minimum value and $X_{\max}$ is the maximum value.

3. Results and discussion

3.1. Analysis of CCD

In order to design a systematic series of experiments (30 runs) in five levels, CCD under RSM was employed. RSM made it feasible to model the experimental data nonlinearly [39–41]. Not only did the CCD avoid running unnecessary experiments but also was beneficial for understanding the synergies among the variables and supply value about interaction between the parameters.

$$R\%\ \text{Purpurin} = 99.393 - 0.66125X_1 - 0.36708X_2 + 0.47708X_3 + 0.27687X_1X_2 + 0.00062500X_2X_3 + 0.0081250X_3X_4 \quad (4)$$

In this equation, the positive values corresponding to each term are indications of their positive effect on response while their negative values show a decrease in the response following raising their value. ANOVA as a statistical method partitions the total variation into its parts while each term has different source of variation. As the results are shown in Table 3, the estimation of interaction effects was easily done by usual ANOVA, while the estimation of factor effect and Fisher's F-ratios and P-values were based on sum of the squares. The model F-value of 12.073 was considered statistically significant and indicated that there was only 0.01% of the chance that "model F-value" could be due to the noise. The insignificant value of lack of fit (more than 0.05) represented validity of the quadratic model for explanation of experimental data of the current study [42]. In order to optimize the adsorption process, the profile for predicted values and desirability option (not shown) was employed. Profiling the desirability of response involved stating the desirability function for R% purpurin as dependent variable by determining the predicted R% purpurin values. For obtaining a comprehensive function that should be

Table 3
The results of ANOVA for the response surface quadratic model of purpurin adsorption.

Source of variation	Df	Purpurin dye			
		Sum of square	Mean square	*F*-value	*P*-value
Model	4	24.932	1.7808	12.073	<0.0001
X_1	1	10.494	10.494	71.145	<0.0001
X_2	1	3.2340	3.2340	21.925	0.00029477
X_3	1	5.4626	5.4626	37.034	<0.0001
X_4	1	0.31970	0.31970	2.1674	0.16163
X_1X_2	1	1.2266	1.2266	7.7982	0.013664
X_1X_3	1	1.1503	1.1503	0.54105	0.47334
X_1X_4	1	0.079806	0.079806	4.2372E-005	0.99489
X_2X_3		6.2500E-006	6.2500E-006	4.9271	0.042274
X_2X_4	1	0.72676	0.72676	0.0071609	0.93368
X_3X_4	1	0.0010563	0.0010563	8.1761	0.011937
X_1^2	1	1.2060	1.2060	0.24016	0.63118
X_2^2	1	0.035424	0.035424	2.0379	0.17390
X_3^2	1	0.30060	0.30060	3.4047	0.084845
X_4^2	1	0.50220	0.50220		
Residual	15	2.2125	0.14750	0.23715	0.97465
Lack of fit	10	0.71181	0.071181		
Pure error	5	1.5007	0.30015		
Correlation total	29	27.144			
Standard Deviation		0.38	R^2	0.9185	
Mean		99.22	Adjusted R^2	0.8424	
Coefficient of Variation (%)		0.39	Predicted R^2	0.7693	
PRESS		6.26	Adequate precision	13.117	

maximized based on the efficient selection and optimization of designed variables, the scale in the range of undesirable (0.0) to very desirable (1.0) was employed. Based on the CCD design matrix results (Table 1), the maximum and minimum of *R*% purpurin were 100.00% and 65.00%, respectively. Concerning this range, the optimum condition at which the highest response can be attained was obtained. The maximum restoration of 99.50% was acquired at optimum conditions regarding these calculations and desirability score of 1.0. For the factors including purpurin concentration, adsorbent dosage, pH, and sonication time, the optimal values were estimated to be 24 mg L^{-1}, 0.027 g, and 4.0 min, respectively. By providing these conditions, 99.48% was predicted to be obtained for *R*% purpurin with desirability of 1.0. Additionally, by performing three experiments at similar conditions, the validity of the predicted response at optimum conditions was inspected. Notably, the obtained experimental response was 99.30%, which was in excellent consistency with the predicted value.

3.2. Modeling of ultrasonic-assisted adsorption process by ANN

The three functions of weight (training), net input, and transfer (tansig) governed the performance of the network. A mean square error (MSE) of 0.0815 was detected at epoch numbers 7 for removal of purpurin dye. At this point, training was stopped and weights have been frozen for the network undergoing testing phase. In Fig. 1, the MSE versus

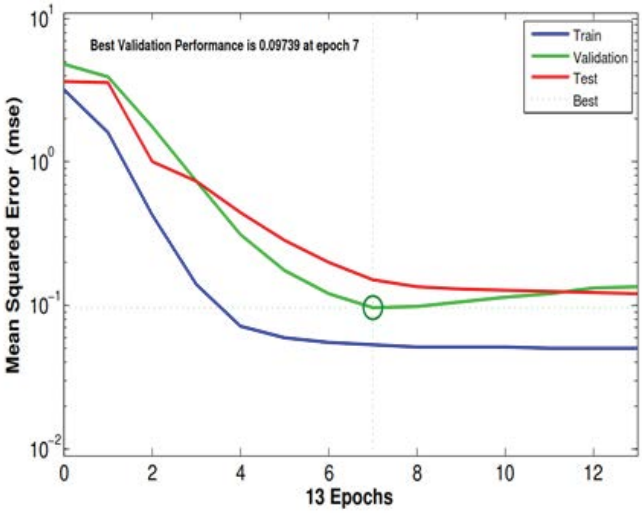

Fig. 1. Evolution of training, validation, and test errors as a function of the number of training epochs during ANN for the purpurin removal by Mn–Fe_2O_4–NPs–AC.

the number of epochs for optimal ANN model is shown. It is observed that the training was stopped after epoch numbers 7 for ultrasonic-assisted removal of purpurin dye. Also in Fig. 1, the reduction of the MSE throughout the training

process is demonstrated. In addition, in Fig. 2, the plot of error histogram for adsorption process is demonstrated indicating that the errors in this removal process are very low. During the net training process in this study, the MSE based on the function of error performance showed minimum value at 5 neurons. A 4–5–1 ANN model with four input layers (viz., initial purpurin dye concentration, adsorbent dosage, pH, and ultrasonic time) based on the output layers (removal of target compounds) was found to be adequately accurate for predicting and estimating the purpurin removal with MSE of 0.0528, 0.1517, and 0.0973 for train, test, and validation, respectively, and the correlation coefficients (R^2) of 0.9689, 0.9057, and 0.9708 for train, test, and validation, respectively (Table 4), for ultrasonic-assisted removal of purpurin dye.

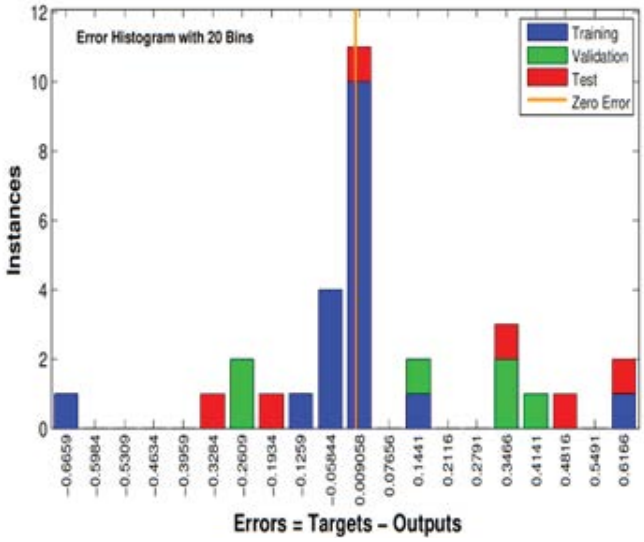

Fig. 2. The plot of error histogram for removal process.

3.3. Three-dimensional response surfaces and contour plots

In order to show the combined effects and discern the major interactions between variables on *R*% of understudy purpurin, the 3-dimensional (3D) response surface plots were employed. In the current study, two 3D response surface plots are demonstrated in Fig. 3. The removal percentage versus the adsorbent dosage is shown in Fig. 3(a), the purpurin removal percentage and adsorbent mass, a positive increase is observed. At lower amount of Mn–Fe_2O_4–NPs–AC, the significant reduction in removal percentage is ascribed to higher ratio of purpurin molecules to the vacant sites of the adsorbent. In Fig. 3(b), the impact of contact time on the purpurin removal percentage is demonstrated. As it is observed, the highest purpurin adsorption could be obtained in short sonication time, which strongly confirms the greater contribution of ultrasound power in mass transfer and accordingly the greater efficiency for the adsorption of purpurin.

3.4. Adsorption isotherms

Based on the assumptions displayed in Table 5, the studied experimental equilibrium data of adsorption of purpurin dye were fitted to conventional isotherms like Langmuir, Freundlich, Temkin, and Dubinin–Radushkevich [43–46]. According to this table, the appropriateness of Langmuir model in interpreting the experimental data indicated that the adsorption of purpurin dye under study was limited to monolayer coverage and the surface was relatively homogenous in terms of interaction of functional groups with purpurin molecule. The maximum adsorption capacity for purpurin on the Mn–Fe_2O_4–NPs–AC was 60 mg g^{-1}.

3.5. Kinetic study

The prediction of adsorption kinetics is crucial since the rate and mechanism of adsorption can be determined based on kinetic studies. The correlation of experimental kinetic data

Table 4
Comparison of 1–15 neurons in the hidden layer for purpurin dye removal by ANN model development with the Levenberg–Marquardt algorithm

Neurons	MSE_{train}	MSE_{test}	$MSE_{validation}$	MSE	R^2_{train}	R^2_{test}	$R^2_{validation}$	R^2
1	0.06931206	0.52012881	0.4743308	0.240479	0.93866424	0.728123187	0.839175753	0.863305996
2	0.65350843	0.74526249	0.1374893	0.568655	0.840447912	0.648034347	0.96153333	0.793319504
3	0.26667503	0.38386246	0.64599	0.365976	0.835721699	0.960104303	0.76722858	0.818855689
4	0.17726547	0.50510765	0.8745432	0.382289	0.856185694	0.848476671	0.781798966	0.814418096
5	0.05286432	0.15178964	0.0973904	0.081555	0.968934752	0.905759435	0.970842175	0.956236076
6	0.17658055	0.50096734	1.1470838	0.435559	0.943115283	0.656829902	0.597838293	0.767555068
7	0.11429439	0.16724061	0.161999	0.134425	0.940216966	0.962671443	0.912749932	0.932584422
8	0.05371092	0.64326218	0.5231746	0.265514	0.96670086	0.71191955	0.844184164	0.844742146
9	0.13121151	1.02121596	0.34684	0.352338	0.943469998	0.278532772	0.689112276	0.80094537
10	0.56968275	0.55756652	0.4521265	0.543748	0.785908891	0.768153736	0.790835006	0.756822379
11	0.09675521	0.21257808	0.3219143	0.164952	0.957438366	0.720331592	0.482669922	0.906576313
12	0.37861645	0.37437045	0.3134466	0.364733	0.790741377	0.81013843	0.79945335	0.790001939
13	0.03133704	0.66415528	0.7204729	0.295728	0.984205216	0.661397183	0.13584398	0.82317805
14	0.31295234	1.63317924	0.1869746	0.551802	0.746142687	0.03849139	0.940179736	0.686838269
15	0.29738354	0.3510409	0.5058606	0.34981	0.900472129	0.316197183	0.159898651	0.786608016

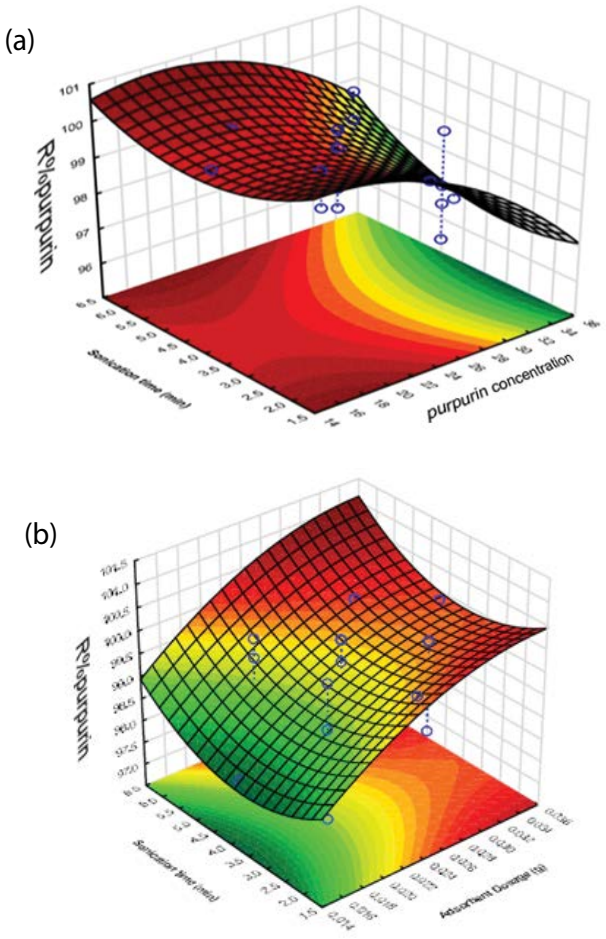

Fig. 3. Response surfaces for the CCD: (a) sonication time – purpurin concentration and (b) sonication time – adsorbent dosage.

Table 6
Kinetic parameters for the adsorption of purpurin onto Mn–Fe_2O_4–NPs–AC

Model	parameters	Value of parameters for purpurin
Pseudo-first-order kinetic	k_1 (min^{-1})	0.677
	q_e (calc) (mg g^{-1})	9.183
	R^2	0.972
pseudo-second-order kinetic	k_2 (min^{-1})	0.124
	q_e (cal) (mg g^{-1})	45.45
	R^2	0.999
Intraparticle diffusion	k_{diff} (mg g^{-1} $min^{-1/2}$)	3.72
	C (mg g^{-1})	35.07
	R^2	0.974
Elovich	β (g mg^{-1})	0.375
	α (mg g^{-1} min^{-1})	65
	R^2	0.972

of purpurin with pseudo-first and second orders, Elovich, and intraparticle diffusion [47–50] was estimated at different sonication time (0.5–5 min). In Table 6, the summary of properties and equation of each model are provided. In comparison with the pseudo-first-order equation, the regression coefficient (R^2) from pseudo-second-order rate equation for adsorbent was higher. These results revealed that the kinetics of purpurin onto adsorbent exhibited best fit to the pseudo-second-order equation for purpurin dye by Mn–Fe_2O_4–NPs–AC.

4. Conclusion

The influences of important variables like initial purpurin dye concentration, pH, adsorbent dosage, and sonication time on the efficiency of removal process were investigated

Table 5
Various isotherm constants and their correlation coefficients calculated for the adsorption of purpurin onto Mn–Fe_2O_4–NPs–AC

Isotherm	Equation	parameters	Value of parameters for purpurin
Langmuir	$q_e = \frac{q_m b C_e}{(1+bC_e)}$	Q_m (mg g^{-1})	120.0
		K_a (L mg^{-1})	0.240
		R^2	0.999
Freundlich	$\ln q_e = \ln K_F + \left(\frac{1}{n}\right)\ln C_e$	$1/n$	0.639
		K_F (L mg^{-1})	4.950
		R^2	0.980
Tempkin	$q_e = B_1 \ln K_T + B_1 \ln C_e$	B_1	30.28
		K_T (L mg^{-1})	5.390
		R^2	0.978
Dubinin–Radushkevich (DR)	$\ln q_e = \ln Q_s - B\,\varepsilon^2$	Q_s (mg g^{-1})	70.19
		$B \times 10^{-7}$	–1.000
		E (kj mol^{-1})	2,272
		R^2	0.973

by CCD. The ANN model was used for building up an empirical model, and the obtained results revealed that the ANN model was a powerful tool for prediction of understudy dye adsorption by Mn–Fe_2O_4–NPs–AC. Eventually, it was observed that the equilibrium of adsorption process followed the Langmuir isotherm. Based on the Langmuir isotherm, at optimum conditions, the highest monolayer capacity (q_{max}) was estimated to be 60 mg g^1 for purpurin removal onto Mn–Fe_2O_4–NPs–AC. In addition, the kinetic models to describe experimental data points at various initial concentrations of adsorbate show that can be successfully fitted to the pseudo-second-order kinetic model. The optimized method was successfully applied to real wastewater samples.

Acknowledgements

The authors gratefully acknowledge partial support of this work by the authors gratefully acknowledge the financial support from the Payame Noor University, Branch of Busher, Iran.

References

[1] S. Mosleh, M. Rahimi, M. Ghaedi, K. Dashtian, Sono-photocatalytic degradation of trypan blue and vesuvine dyes in the presence of blue light active photocatalyst of Ag 3 PO 4/Bi 2 S 3-HKUST-1-MOF: central composite optimization and synergistic effect study, Ultrason. Sonochem., 32 (2016) 387–397.
[2] M. Panizza, M.A. Oturan, Degradation of Alizarin Red by electro-Fenton process using a graphite-felt cathode, Electrochim. Acta, 56 (2011) 7084–7087.
[3] J. García-Montaño, X. Domenech, J.A. García-Hortal, F. Torrades, J. Peral, The testing of several biological and chemical coupled treatments for Cibacron Red FN-R azo dye removal, J. Hazard. Mater., 154 (2008) 484–490.
[4] E.H. Koupaie, M.A. Moghaddam, S. Hashemi, Post-treatment of anaerobically degraded azo dye Acid Red 18 using aerobic moving bed biofilm process: enhanced removal of aromatic amines, J. Hazard. Mater., 195 (2011) 147–154.
[5] B.K. Körbahti, K. Artut, C. Geçgel, A. Özer, Electrochemical decolorization of textile dyes and removal of metal ions from textile dye and metal ion binary mixtures, Chem. Eng. J., 173 (2011) 677–688.
[6] E. Alventosa-deLara, S. Barredo-Damas, M. Alcaina-Miranda, M. Iborra-Clar, Ultrafiltration technology with a ceramic membrane for reactive dye removal: optimization of membrane performance, J. Hazard. Mater., 209 (2012) 492–500.
[7] G. Zhang, L. Yi, H. Deng, P. Sun, Dyes adsorption using a synthetic carboxymethyl cellulose-acrylic acid adsorbent, J. Environ. Sci., 26 (2014) 1203–1211.
[8] M.J. Sweet, A. Chessher, I. Singleton, Metal-based Nanoparticles; Size, Function, and Areas for Advancement in Applied Microbiology, in: Advances in Applied Microbiology, Elsevier, 2012, pp. 113–142.
[9] T. Okada, J. Suehiro, Synthesis of nano-structured materials by laser-ablation and their application to sensors, Appl. Surf. Sci., 253 (2007) 7840–7847.
[10] Y. Chen, Synthesis, characterization and dye adsorption of ilmenite nanoparticles, J. Non-Cryst. Solids, 357 (2011) 136–139.
[11] M. Faraji, Y. Yamini, M. Rezaee, Magnetic nanoparticles: synthesis, stabilization, functionalization, characterization, and applications, J. Iran. Chem. Soc., 7 (2010) 1–37.
[12] G. Absalan, M. Asadi, S. Kamran, L. Sheikhian, D.M. Goltz, Removal of reactive red-120 and 4-(2-pyridylazo) resorcinol from aqueous samples by Fe_3O_4 magnetic nanoparticles using ionic liquid as modifier, J. Hazard. Mater., 192 (2011) 476–484.
[13] M.R.P.V. Shrivastava, Adsorption removal of carcinogenic acid violet19 dye from aqueous solution by polyaniline-Fe_2O_3 magnetic nano-composite, J. Mater. Environ. Sci., 6 (2015) 11–21.
[14] W. Song, M. Liu, R. Hu, X. Tan, J. Li, Water-soluble polyacrylamide coated-Fe_3O_4 magnetic composites for high-efficient enrichment of U (VI) from radioactive wastewater, Chem. Eng. J., 246 (2014) 268–276.
[15] E.A. Dil, M. Ghaedi, A. Asfaram, F. Mehrabi, Application of modificated magnetic nanomaterial for optimization of ultrasound-enhanced removal of Pb^{2+} ions from aqueous solution under experimental design: investigation of kinetic and isotherm, Ultrason. Sonochem., 36 (2017) 409–419.
[16] F.N. Azad, M. Ghaedi, A. Asfaram, A. Jamshidi, G. Hassani, A. Goudarzi, M.H.A. Azqhandi, A. Ghaedi, Optimization of the process parameters for the adsorption of ternary dyes by Ni doped FeO (OH)-NWs–AC using response surface methodology and an artificial neural network, RSC Adv., 6 (2016) 19768–19779.
[17] A.R. Bagheri, M. Ghaedi, A. Asfaram, S. Hajati, A.M. Ghaedi, A. Bazrafshan, M.R. Rahimi, Modeling and optimization of simultaneous removal of ternary dyes onto copper sulfide nanoparticles loaded on activated carbon using second-derivative spectrophotometry, J. Taiwan Inst. Chem. Eng., 65 (2016) 212–224.
[18] A. Asfaram, M. Ghaedi, S. Hajati, A. Goudarzi, E.A. Dil, Screening and optimization of highly effective ultrasound-assisted simultaneous adsorption of cationic dyes onto Mn-doped Fe_3O_4-nanoparticle-loaded activated carbon, Ultrason. Sonochem., 34 (2017) 1–12.
[19] M.S. Tehrani, R. Zare-Dorabei, Competitive removal of hazardous dyes from aqueous solution by MIL-68 (Al): derivative spectrophotometric method and response surface methodology approach, Spectrochim. Acta A Mol. Biomol. Spectrosc., 160 (2016) 8–18.
[20] A.R. Bagheri, M. Ghaedi, A. Asfaram, R. Jannesar, A. Goudarzi, Design and construction of nanoscale material for ultrasonic assisted adsorption of dyes: application of derivative spectrophotometry and experimental design methodology, Ultrason. Sonochem., 35 (2017) 112–123.
[21] E.A. Dil, M. Ghaedi, A. Ghaedi, A. Asfaram, A. Goudarzi, S. Hajati, M. Soylak, S. Agarwal, V.K. Gupta, Modeling of quaternary dyes adsorption onto ZnO–NR–AC artificial neural network: analysis by derivative spectrophotometry, J. Ind. Eng. Chem., 34 (2016) 186–197.
[22] M.S. Tehrani, R. Zare-Dorabei, Highly efficient simultaneous ultrasonic-assisted adsorption of methylene blue and rhodamine B onto metal organic framework MIL-68 (Al): central composite design optimization, RSC Adv., 6 (2016) 27416–27425.
[23] E.A. Dil, M. Ghaedi, A. Asfaram, F. Zare, F. Mehrabi, F. Sadeghfar, Comparison between dispersive solid-phase and dispersive liquid–liquid microextraction combined with spectrophotometric determination of malachite green in water samples based on ultrasound-assisted and preconcentration under multi-variable experimental design optimization, Ultrason. Sonochem., 39 (2017) 374–383.
[24] M. Dastkhoon, M. Ghaedi, A. Asfaram, M.H.A. Azqhandi, M.K. Purkait, Simultaneous removal of dyes onto nanowires adsorbent use of ultrasound assisted adsorption to clean waste water: chemometrics for modeling and optimization, multicomponent adsorption and kinetic study, Chem. Eng. Res. Des., 124 (2017) 222–237.
[25] A. Asfaram, M. Ghaedi, F. Yousefi, M. Dastkhoon, Experimental design and modeling of ultrasound assisted simultaneous adsorption of cationic dyes onto ZnS: Mn-NPs-AC from binary mixture, Ultrason. Sonochem., 33 (2016) 77–89.
[26] A. Asfaram, M. Ghaedi, M.A. Azqhandi, A. Goudarzi, M. Dastkhoon, Statistical experimental design, least squares-support vector machine (LS-SVM) and artificial neural network (ANN) methods for modeling the facilitated adsorption of methylene blue dye, RSC Adv., 6 (2016) 40502–40516.
[27] N. Khan, T.G. Kazi, M. Tuzen, M. Soylak, A multivariate study of solid phase extraction of beryllium (II) using human hair as adsorbent prior to its spectrophotometric detection, Desal. Wat. Treat., 55 (2015) 1088–1095.

[28] A. Asfaram, M. Ghaedi, M.K. Purkait, Novel synthesis of nanocomposite for the extraction of Sildenafil Citrate (Viagra) from water and urine samples: process screening and optimization, Ultrason. Sonochem., 38 (2017) 463–472.
[29] F. Mehrabi, E.A. Dil, Investigate the ultrasound energy assisted adsorption mechanism of nickel (II) ions onto modified magnetic cobalt ferrite nanoparticles: multivariate optimization, Ultrason. Sonochem., 37 (2017) 37–46.
[30] E.A. Dil, M. Ghaedi, A. Asfaram, A.A. Bazrafshan, Ultrasound wave assisted adsorption of congo red using gold-magnetic nanocomposite loaded on activated carbon: optimization of process parameters, Ultrason. Sonochem., 46 (2018) 99–105.
[31] A. Asfaram, M. Ghaedi, H. Abidi, H. Javadian, M. Zoladl, F. Sadeghfar, Synthesis of Fe_3O_4@ CuS@ Ni_2P-CNTs magnetic nanocomposite for sonochemical-assisted sorption and pre-concentration of trace Allura Red from aqueous samples prior to HPLC-UV detection: CCD-RSM design, Ultrason. Sonochem., 44 (2018) 240–250.
[32] H.Z. Khafri, M. Ghaedi, A. Asfaram, M. Safarpoor, Synthesis and characterization of ZnS: Ni-NPs loaded on AC derived from apple tree wood and their applicability for the ultrasound assisted comparative adsorption of cationic dyes based on the experimental design, Ultrason. Sonochem., 38 (2017) 371–380.
[33] F.N. Azad, M. Ghaedi, K. Dashtian, S. Hajati, V. Pezeshkpour, Ultrasonically assisted hydrothermal synthesis of activated carbon–HKUST-1-MOF hybrid for efficient simultaneous ultrasound-assisted removal of ternary organic dyes and antibacterial investigation: Taguchi optimization, Ultrason. Sonochem., 31 (2016) 383–393.
[34] A. Asfaram, M. Ghaedi, A. Goudarzi, Optimization of ultrasound-assisted dispersive solid-phase microextraction based on nanoparticles followed by spectrophotometry for the simultaneous determination of dyes using experimental design, Ultrason. Sonochem., 32 (2016) 407–417.
[35] A. Asfaram, M. Ghaedi, S. Hajati, A. Goudarzi, Synthesis of magnetic γ-Fe2O3-based nanomaterial for ultrasonic assisted dyes adsorption: modeling and optimization, Ultrason. Sonochem., 32 (2016) 418–431.
[36] S. Bagheri, Application of response surface methodology to modeling and optimization of removal of Bismarck Brown and Thymol Blue by Mn-Fe_2O_4-NPs-AC: kinetics and thermodynamic studies, Orient. J. Chem., 32 (2016) 549–565.
[37] Y. Liu, G. Cui, C. Luo, L. Zhang, Y. Guo, S. Yan, Synthesis, characterization and application of amino-functionalized multi-walled carbon nanotubes for effective fast removal of methyl orange from aqueous solution, RSC Adv., 4 (2014) 55162–55172.
[38] A. Asfaram, M. Ghaedi, S. Hajati, A. Goudarzi, A.A. Bazrafshan, Simultaneous ultrasound-assisted ternary adsorption of dyes onto copper-doped zinc sulfide nanoparticles loaded on activated carbon: optimization by response surface methodology, Spectrochim. Acta A Mol. Biomol. Spectrosc., 145 (2015) 203–212.
[39] E.A. Dil, M. Ghaedi, A. Ghaedi, A. Asfaram, M. Jamshidi, M.K. Purkait, Application of artificial neural network and response surface methodology for the removal of crystal violet by zinc oxide nanorods loaded on activate carbon: kinetics and equilibrium study, J. Taiwan Inst. Chem. Eng., 59 (2016) 210–220.
[40] P. Hashemi, S. Beyranvand, R.S. Mansur, A.R. Ghiasvand, Development of a simple device for dispersive liquid–liquid microextraction with lighter than water organic solvents: isolation and enrichment of glycyrrhizic acid from licorice, Anal. Chim. Acta, 655 (2009) 60–65.
[41] M. Ghaedi, A. Shahamiri, S. Hajati, B. Mirtamizdoust, A novel PVC-membrane optical sensor for high sensitive and selective determination of Cu^{2+} ion based on synthesized (E)-N′-(pyridin-2-ylmethylene) isonicotin-ohydrazide, J. Mol. Liq., 199 (2014) 483–488.
[42] S.-Y. Jeong, J.-W. Lee, Optimization of pretreatment condition for ethanol production from oxalic acid pretreated biomass by response surface methodology, Ind. Crops. Prod., 79 (2016) 1–6.
[43] I. Langmuir, The adsorption of gases on plane surfaces of glass, mica and platinum, J. Am. Chem. Soc., 40 (1918) 1361–1403.
[44] H. Freundlich, Über die adsorption in lösungen, Zeitschrift für physikalische Chemie, 57 (1907) 385–470.
[45] M. Temkin, V. Pyzhev, Recent modifications to Langmuir isotherms, Acta Phys. 12 (1940) 217–222.
[46] M. Dubinin, V. Serpinsky, Isotherm equation for water vapor adsorption by microporous carbonaceous adsorbents, Carbon, 19 (1981) 402–403.
[47] Y. Ho, J. Ng, G. McKay, Kinetics of pollutant sorption by biosorbents, Sep. Purif. Methods, 29 (2000) 189–232.
[48] Y.-S. Ho, G. McKay, Pseudo-second-order model for sorption processes, Process Biochem., 34 (1999) 451–465.
[49] W.J. Weber, J.C. Morris, Kinetics of adsorption on carbon from solution, J. Sanit. Eng. Div., 89 (1963) 31–60.
[50] F.-C. Wu, R.-L. Tseng, R.-S. Juang, Characteristics of Elovich equation used for the analysis of adsorption kinetics in dye-chitosan systems, Chem. Eng. J., 150 (2009) 366–373.